RESEARCH ARTICLE

The Holocene Secche di Lazzaro phreatomagmatic succession (Stromboli, Italy): evidence of pyroclastic density current origin deduced by facies analysis and AMS flow directions

**Guido Giordano · Massimiliano Porreca ·
Pietro Musacchio · Massimo Mattei**

Abstract The edifice of Stromboli volcano gravitationally collapsed several times during its volcanic history (>100 ka–present). The largest Holocene event occurred during the final stage of the Neostromboli activity (~13–5 ka), and was accompanied by the emplacement of phreatomagmatic and lahar deposits, known as the Secche di Lazzaro succession. A stratigraphic and paleomagnetic study of the Secche di Lazzaro deposits allows the interpretation of the emplacement and the eruptive processes. We identify three main units within the succession that correspond to changing eruption conditions. The lower unit (UA) consists of accretionary lapilli-rich, thinly bedded, parallel- to cross-stratified ash deposits, interpreted to indicate the early stages of the eruption and emplacement of dilute pyroclastic density currents. Upward, the second unit (UB) of the deposit is more massive and the beds thicker, indicating an increase in the sedimentation rate from pyroclastic density currents. The upper unit (UC) caps the succession with thick, immediately post-eruptive lahars, which reworked ash deposited on the volcano's slope. Flow directions obtained by Anisotropy of Magnetic Susceptibility (AMS) analysis of the basal bed of UA at the type locality suggest a provenance of pyroclastic currents from the sea. This is interpreted to be related to the initial base-surges associated with water–magma interaction that occurred

immediately after the lateral collapse, which wrapped around the shoulder of the sector collapse scar. Upward in the stratigraphy (upper beds of UA and UB) paleoflow directions change and show a provenance from the summit vent, probably related to the multiple collapses of a vertical, pulsatory eruptive column.

Introduction

Stromboli volcano is characterised by persistent mild "Strombolian" explosive activity for at least the past 1000 yrs (Rosi et al. 2000). This "normal" activity is periodically interrupted by eruptive crises that are either lava emission and/or violent short-lived explosions (e.g. the 5th April 2003 paroxysmal event), which may or may not be associated with partial collapses of the edifice and generation of tsunamis, both of which occurred during the 2002–2003 eruption (Bonaccorso et al. 2003; Ripepe et al. 2005) and the 2007 eruption (http://www.ingv.it). These crises have occurred in the last century with an average frequency of one every 5–15 years, the most intense being the 1930 eruption when pyroclastic flows were also generated (Barberi et al. 1993), and are recorded also in the stratigraphy of the last millennia (e.g. Speranza et al. 2004).

However, the most dangerous scenario at Stromboli is associated with the lateral sector collapse of the volcano, fortunately a less frequent event that has nevertheless occurred several times and is recorded in the geology by

G. Giordano · M. Porreca · P. Musacchio · M. Mattei
Dipartimento Scienze Geologiche, Università Roma Tre,
Rome, Italy

G. Giordano (✉) · M. Porreca · P. Musacchio · M. Mattei
Largo S. Leonardo Murialdo 1,
00154 Roma, Italia
e-mail: giordano@uniroma3.it

several large scars perpendicular to the NE elongation of the island (e.g. Tibaldi 2001). The last major volcanotectonic collapse occurred during the final stage of Neostromboli activity at ~5 ka (Gillot and Keller 1993), which decapitated the volcano, producing the NE-facing Sciara del Fuoco scar, wherein the present day activity is confined.

The phreatomagmatic Secche di Lazzaro (SDL) pyroclastics were interpreted by Bertagnini and Landi (1996) as the product of the lateral sector collapse of the Neostromboli volcano, which allowed access of sea water to the volcanic conduit and triggered a large phreatomagmatic eruption. Previously the SDL pyroclastics were interpreted as erupted from a phreatomagmatic centre located offshore (Hornig-Kjarsgaard et al. 1993). The SDL pyroclastics are best exposed on the SW slope of the island (Fig. 1), but are poorly exposed and are in outcrop only in a few scattered localities on the N and S slope of the volcano, and have not yet been described in detail. The phreatomagmatic origin of the SDL deposits is also proved by the very low emplacement temperatures defined by paleomagnetic data (Porreca et al. 2006).

The main problem in reconstructing the eruptive scenario associated with the lateral sector collapse at Stromboli is that, in contrast to cases of lateral sector collapse in subaerial environment (e.g. 18th May 1980 at Mount St. Helens; Christiansen and Peterson 1981; 1956 at Bezymianny; Bogoyavlenskaya et al. 1985), the deposits of the collapse and the following explosive activity are mostly submarine.

This detailed stratigraphic-sedimentological and magnetic fabric study is aimed at clarifying the origin of the SDL

pyroclastic succession and its likely relationship to the lateral sector collapse of the volcano.

Flow directions obtained by the analysis of the magnetic fabric for the basal part of SDL deposits at the type locality (that is near Ginostra village, behind the shoulder of the Sciara del Fuoco sector collapse rim) indicate an early provenance of pyroclastic density currents from the sea, which we interpret as related to the initial lateral sector collapse, which spread around the shoulder of the sector collapse scar, similar to the occurrences described for the 1902 eruption at Montagne Peleé in Martinique (Fisher and Heiken 1982). Up through stratigraphy, paleoflow directions change and show a provenance from the summit vent, which we interpret as related to the pulsatory collapse of a vertical eruptive column, established after the lateral collapse.

Geological setting

Stromboli is the northernmost island of the Aeolian volcanic arc, located in the southern Tyrrhenian Sea. The Aeolian volcanic arc is ~200 km long and consists of seven main islands (Alicudi, Filicudi, Salina, Lipari, Vulcano, Panarea and Stromboli; inset in Fig. 1), and several submarine volcanoes occurring above a north-westward-dipping Benioff zone elongated in a NE–SW direction with a maximum depth of 500 km (Ferrari and Manetti 1993; Selvaggi and Chiarabba 1995). Volcanic activity started at ~800 ka (De Astis et al. 2003) with magmatism ranging from CA, HKCA and shoshonitic with unclear temporal trends; volcanic activity is still persistent at Stromboli.

The island of Stromboli at 924 m a.s.l. in elevation is the subaerial part of a stratovolcano, which rises 3000 m above the seafloor base (Gabbianelli et al. 1993) and is elongated NE. The oldest product in outcrop is the Strombolicchio islet (204±25 ka; Gillot and Keller 1993), a neck located approximately 2 km NE of the main island (Rosi 1980). Deposits on the main island are younger than 100 ka (Gillot and Keller 1993).

The stratigraphy has been subdivided into seven superposed edifices, according to major stratigraphic unconformities: Paleostromboli I (100–64 ka; HKCA), Paleostromboli II (64–55 ka; CA), Paleostromboli III (<55–35 ka; HKCA to shoshonitic), Scari (35 ka; shoshonitic), Vancori (>25–13 ka; shoshonitic), Neostromboli (13–5 ka; KS) and Recent Stromboli (<5 ka–Present; shoshonitic, HKCA) (Hornig-Kjarsgaard et al. 1993).

The volcano-tectonic lateral sector collapse of the NE sector of the volcano, which created the Sciara del Fuoco scar, was produced at the end of the Neostromboli period (Hornig-Kjarsgaard et al. 1993; Pasquaré et al. 1993; Tibaldi 2001). The scar extends approximately 1700 m
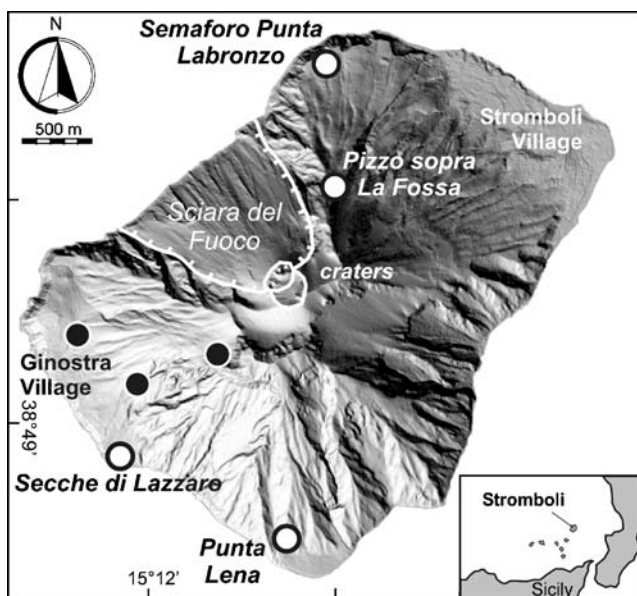

Fig. 1 Geological sketch map of Stromboli and location of the outcrops of the Secche di Lazzaro (SDL) pyroclastics. *White dots* refer to sections described and analysed in this work; *black dots* refer to other outcrops from Bertagnini and Landi (1996)

under the sea and is partially buried by the products of the recent eruptive activity (Romagnoli et al. 1993; Kokelaar and Romagnoli 1995). The present strombolian and effusive activity of the volcano is focussed within the Sciara del Fuoco.

Stratigraphy and facies of the Secche di Lazzaro pyroclastics

The Secche di Lazzaro phreatomagmatic succession crops out at various scattered locations on the island of Stromboli (Fig. 1; cf. Bertagnini and Landi 1996). The best exposures are at type locality Secche di Lazzaro (SW flank), at Punta Lena (S flank), at Semaforo Punta Labronzo and at 380 m a.s.l. on the path toward Pizzo sopra la Fossa (N flank). The stratigraphy of the succession has been briefly described only from its type locality in Hornig-Kjarsgaard et al. (1993), Bertagnini and Landi (1996) and Porreca et al. (2006). Both Hornig-Kjarsgaard et al. (1993) and Bertagnini and Landi (1996) interpreted the succession as the interlayering of thinly bedded, accretionary lapilli-rich fallout deposits and massive and chaotic, debris- to mud-flow lahar deposits. The juvenile component of SDL is sparsely porphyritic (clinopyroxene+olivine+plagioclase+apatite+oxide+biotite), light coloured, highly vesicular pumice lapilli, Lc-shoshonitic (potassic series, KS) in composition (Bertagnini and Landi 1996). The xenolithic component is made of multilithologic lava fragments including hydrothermally altered clasts which indicate the presence of a shallow hydrothermal system beneath the vent (Bertagnini and Landi 1996).

In order to interpret the depositional processes associated with the eruption of SDL, each important outcrop on the island is described below.

Secche di Lazzaro/Ginostra

This is the type locality for the succession. Total thickness varies between 4 and 8 m (Fig. 2a, b); SDL overlies loose blocks of Neostromboli lava that formed a paleobeach at the time of the emplacement. The outcrop offers a section >400 m long parallel to the coast and also a perpendicular 50 m long section along slope. The succession can be subdivided, based on the facies characteristics, into three units: UA, UB and UC (Fig. 2b).

UA constitutes the basal portion of the stratigraphic succession and is comprised of 11 beds (UA0–UA10) with an overall tabular geometry and a dominant parallel- to cross-stratified lithofacies.

UA0 is a massive to weakly stratified, matrix-supported deposit, with abundant accretionary lapilli, equant and generally smaller than 0.5 cm in diameter. Ash composes 95% of the deposit, is yellow in colour, and consists of blocky glass shards (∼50%), crystals fragments and small lithic clasts. Rare centimetre-sized multilithologic lava lithic clasts are mixed with the ash. Commonly, the accretionary lapilli are not dispersed in the ash matrix, but form a clast supported accretionary-lapilli deposit (Fig. 3a). The important characteristic of UA0 is that rather that being a continuous bed, it fills the empty spaces between blocks on the paleobeach of Neostromboli down to half a metre below the top of the blocks (Fig. 3a,b). Prints of unburnt

Fig. 2 **a** The Secche di Lazzaro (SDL) pyroclastics at type locality. The *picture* shows part of a 150 m long outcrop. Lava blocks at the base represent the paleobeach of Neostromboli lava, overlain by the stratified UA, the massive UB and the lithic-rich lahar of UC (see text for explanation); **b** schematic stratigraphic log of SDL pyroclastics

Fig. 3 **a** Deposit of UA0 composed of massive fine ash and ~0.5 cm accretionary lapilli. Note the presence of cane moulds and the presence of a matrix-depleted, accretionary-lapilli supported agglomerate. UA0 fills holes in between the lava blocks of the paleobeach over which the SDL pyroclastics were emplaced; **b** progradational dune formed by the *UA1–UA10* beds at SDL locality. Flow direction from *left-inside* the photo to *right-outward*, i.e. from *N* to *S*; **c** UA of the SDL pyroclastics is made by a succession of thin beds (here *UA1–UA5*) individually formed by a distinct couplet of layers: the basal layer, made of grey coarse ash, with internal faint low angle cross-stratification; the *top layer*, massive, with abundant accretionary lapilli. The overall lithofacies is parallel-stratified to low angle cross-stratified
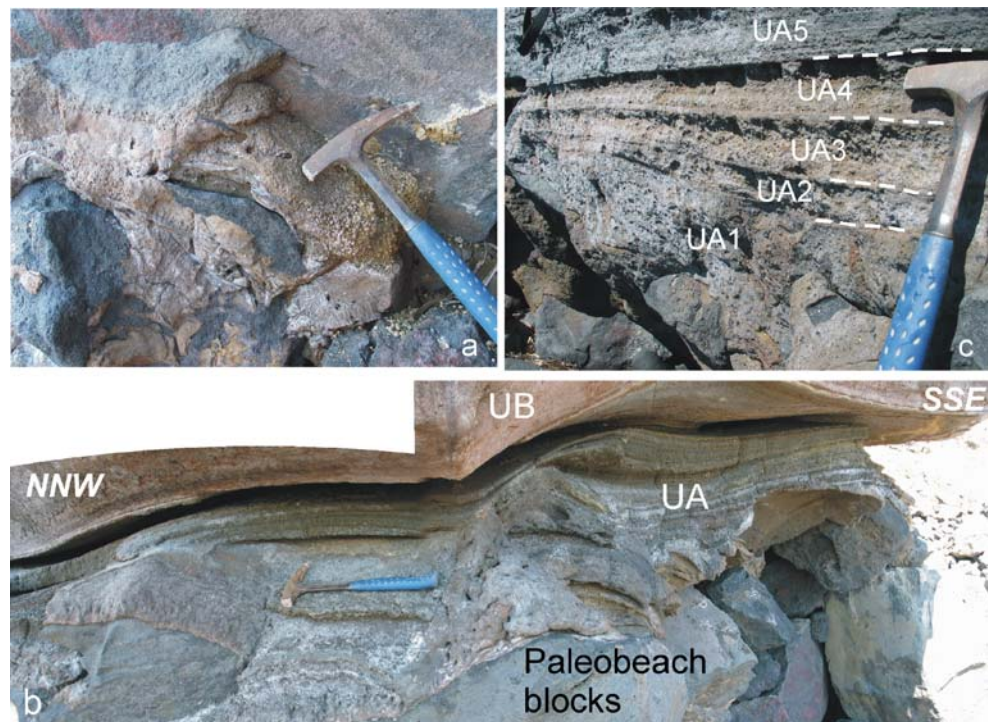
cane pieces are commonly admixed with accretionary lapilli and ash (Fig. 3a).

UA1–UA10 are few—20 cm thick, indurated ash-rich beds with aggradational, plane-parallel to cross-stratification (Fig. 3b,c). The total thickness varies from 60 cm to 130 cm. Thickness variations correspond to different facies, veneer facies where thin and lobe faces where thicker. The ash matrix shows small vugs (henceforth the presence of small vugs in the ash matrix will be referred as "vesiculated ash matrix", cf. "vesiculated tuffs", Lorenz 1974; Rosi 1992), and is bimodal, with the fine fraction made of blocky to weakly vesicular shards (up to 50%), and the coarse fraction made mostly of crystal fragments of

clinopyroxene, plagioclase and biotite and small angular fragments of lava. Lava xenoliths with maximum diameter of 3 cm can be found dispersed in the ash matrix. Each bed of UA1–UA10 is formed by a distinct couplet of layers (Fig. 3c). The basal layer (UA_b) is 1–6 cm thick on average (see the layer $UA5_b$ in Fig. 4a), made of grey ash, with internal faint low angle cross-stratification. The top layers (UA_t) are generally thicker than the basal ones (see the layer $UA5_t$ in Fig. 4a) and can be up to 10 cm thick, massive, with abundant accretionary lapilli (grain size <0.5 cm), which may constitute up to 80% of the layer, the reminder being ash matrix. UA1–10 may have constant thickness laterally for many metres, which is why they have
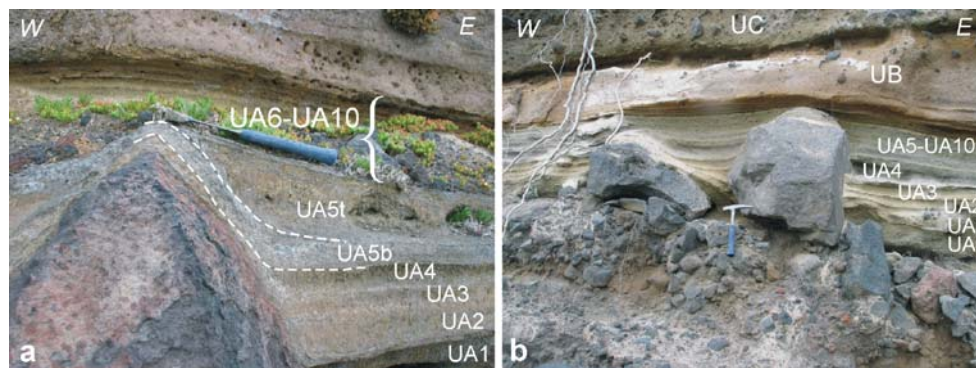

Fig. 4 Ponding of individual layers of UA between boulders of the underlying paleobeach. **a** The accretionary lapilli-rich layers of UA1–UA5 pinch out sharply over the lava boulder filling the paleotopography before the deposition of the overlying plane-parallel UA6–UA10. Note the difference in thickness between $UA5_b$ and $UA5_t$, *basal* and *top layer*, respectively. **b** The UA beds pond between the

two boulders at the *centre* of the photo. The sharp truncations across the vertical face of the right boulder, and the absence of a similar stratigraphy on top of the boulder unequivocally indicate the flow origin of UA. Flow direction from *left*-inside the photo to the *right*-outside the photo

been previously interpreted as fallout beds (cf. Bertagnini and Landi 1996; Hornig-Kjarsgaard et al. 1993). However, several geometric and depositional characteristics clearly indicate an origin from pyroclastic density currents. Beds show lateral thickening and thinning and form dm- to m-scale wavelength dunes, progradational toward the S, i.e. almost orthogonal to the coast (Fig. 3b). Where sharp paleotopographic irregularities were present, such as across the paleobeach lava blocks, beds thin on topographic highs, pond in topographic lows (Fig. 4a,b) and may also show sharp edges across obstacles (Fig. 5a). Both UA_b and UA_t show ponding in topographic lows. However, UA_b tends to better mantle the paleotopography, whereas UA_t shows better defined topographic confinement (Fig. 4a). Furthermore, at several locations, beds wedge under some blocks that appear pushed laterally and imbricated (Fig. 5a). These observations demonstrate the inception of ripping up clasts from the substrate by the pyroclastic density currents (e.g., La Berge et al. 2006).

UA1 and UA5 are characterised by sudden lateral variations of thickness, passing from 5–10 cm (veneer facies) to up to 100 cm (lobe facies, Fig. 5b). The veneer facies is the one just described for UA1–UA10. The lobe facies is matrix-supported, massive and chaotic. The ash-matrix consists of blocky to vesicular shards, crystal fragments of clinopyroxene, biotite and plagioclase and small lava clasts. The ash matrix can be vesiculated and composes up to 80% of the deposit. The coarse fraction is up to 20% of variably oxidised (ranging from black to red), angular, multilithologic lava blocks, up to 1 m in diameter. This abundant and coarse clast population, which is not

present in the veneer facies of the same beds, is likely accidental, i.e. ripped up from the substrate during transport. This is suggested by the presence also of unconsolidated stratified tephra clasts eroded from underlying UA1–UA4 deposits (shown in Fig. 5b). Flame and liquefaction structures are observed in UA1–UA4, produced by the erosional capacity of the UA5 flow and of the dynamic loading exerted by the suddenly emplaced deposit. These thick lobes may be up to 40 m long, have low aspect ratio, with planar base and very open convex upward top (Fig. 5b). Thickening does not correspond to topographic lows and therefore indicates the emplacement of lobes rather than of valley-pond currents. It is likely that the formation of lobes may relate to bulking of the pyroclastic current as accidental clasts are incorporated in the flow, as well as vapour condensation, which favour the transition from a gas/steam supported current to a steam/water supported current.

UA5 contains between 1–5% of light coloured, highly vesicular, sparsely porphyritic (mostly clinopyroxene, plagioclase, biotite and rare olivine) pumice lapilli, with fluidal shape, ranging in size between 1 mm and 2 cm.

UB varies in thickness from 25 cm to 235 cm (Fig. 2a, b). It is matrix-supported, generally massive, from chaotic to diffusely stratified (Fig. 6a). The base is low angle cross-stratified. The deposit is largely grey ash (90–98%), composed of blocky to vesicular shards, crystal fragments of clinopyroxene, biotite and plagioclase, and small multi-lithologic lava fragments. The coarse fraction (2–10%) is made of lapilli- to block-sized multilithologic lava lithic clasts (max 8 cm), accretionary lapilli and armoured lapilli up to 2 cm in diameter. Armoured lapilli are commonly

Fig. 5 a UA at SDL in section parallel to flow direction that is from *right* to *left*. Lava blocks of the paleobeach have been pushed laterally and imbricated. Note that UA1–UA4 are squeezed in at the base of blocks, UA5 is plastered laterally and UA6–UA10 are wrapped on *top*. This organisation suggests that blocks have been lifted up and then laterally pushed. Dimensions (in cm) of blocks 1, 2, 3 are 70×60×50, 110×67×60, 85×60×51, respectively; **b** lobe facies of UA5 with rip-up underlying deposits clasts. Hammer for scale
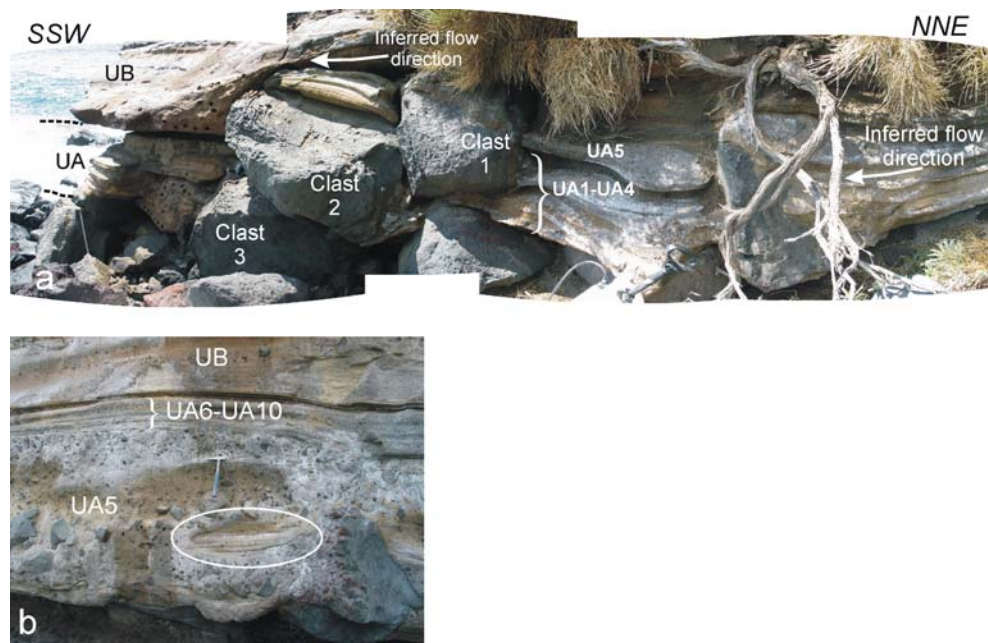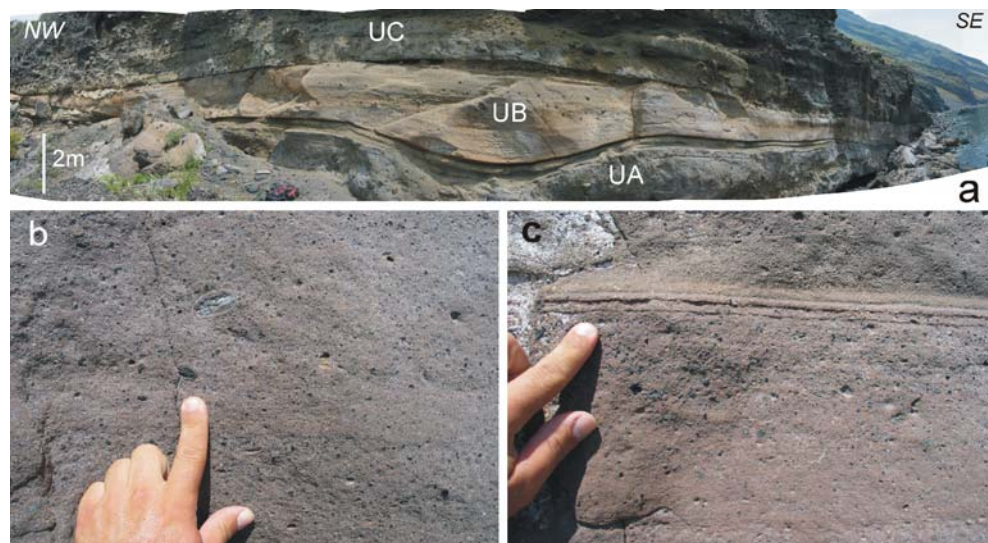
Fig. 6 a Ponding of *UB* in paleotopography at SDL; b *UB* at SDL bears centimetre-sized armoured lapilli and millimetre-to centimetre-sized accretionary lapilli; c UB at SDL shows the presence of interbedded stratified fine ash layers between massive and chaotic to faintly stratified depositional units

wrapped around black scoria xenoliths (Fig. 6b). UB bears rare light-coloured, highly vesicular, sparsely porphyritic (clinopyroxene, plagioclase, biotite and rare olivine) pumice lapilli. Internally, UB shows variation in grainsize, where three subunits (maximum thickness 134+16+85 cm respectively) are separated by the presence of thin layers of fine ash (Fig. 6c), which indicate the pulsatory nature of emplacement. UB is lenticular and valley ponded (Fig. 2a), the base conformably overlies UA10 (Fig. 5b), whereas the top is flat and gently sloping with the topography (Fig. 2a). The geometrical and depositional characteristics of UB, together with the presence of accretionary and armoured lapilli, are consistent with emplacement from a pyroclastic density current (Branney and Kokelaar 2002; Cas and Wright 1987) and not, as previously reported, by lahar (cf. Bertagnini and Landi 1996; Hornig-Kjarsgaard et al. 1993).

UC (Figs. 2a,b and 6a). The top part of Secche di Lazzaro succession is composed of several beds with a total thickness of up to 5 m. Individual beds are 1–2 m thick, indurated, lithic-rich, matrix-supported, massive and chaotic. The dark grey matrix comprises approximately 60–70%

of the deposit and consists of variably hydrated and altered shards, and crystal fragments mostly of clinopyroxene and plagioclase. The coarse fraction is constituted by multi-lithologic lava lithic clasts cm to 1 m in size, and generally with subrounded shapes. The stratigraphic contact with the underlying unit UB is generally planar, but small V-shaped gullies occur and testify to a short timegap between the emplacement of UB and UC. UC is interpreted as immediately post-eruptive lahar deposits.

Punta Lena locality

Punta Lena is the southernmost point of Stromboli (Fig. 1). At this locality, SDL outcrops are confined in a narrow, U-shaped paleo-valley (Fig. 7a) and in scattered outcrops nearby. The valley is approximately 10 m across and inclined seaward at 15°. Valley sides slope up to 50°. The SDL succession shows the same partitioning into UA and UB (Fig. 7a), and UC deposits are absent.

UA is composed of 10 beds, as at the Secche di Lazzaro outcrop, except that the basal bed UA0 is missing. The total

Fig. 7 a SDL pyroclastics at Punta Lena paleovalley locality. Person for scale; b UA1–7 at Punta Lena
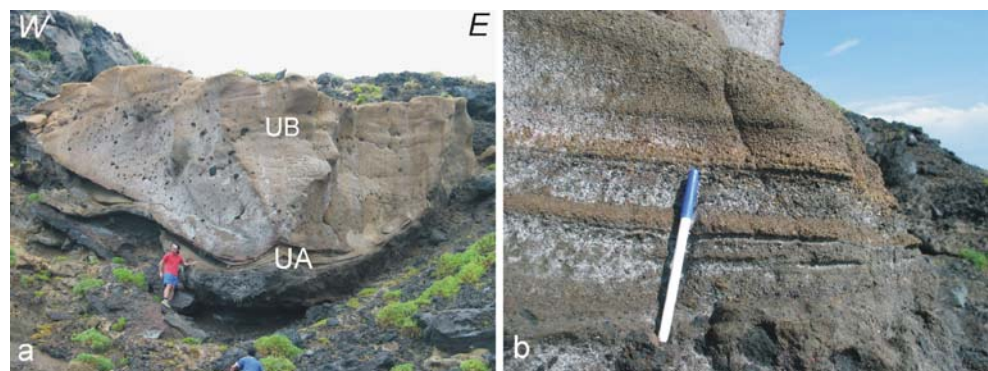
maximum thickness is 160 cm. Individual beds consist of alternating thin, faintly laminated, ash layers and accretionary and armoured lapilli-rich, 2–15 cm-thick layers (Fig. 7b). The ash is composed of blocky to vesicular shards and crystal fragments of clinopyroxene, plagioclase and biotite. Light, highly vesicular, sparsely porphyritic (clinopyroxene, plagioclase, biotite) pumice lapilli are present, especially in UA1 and UA2. Occasional centimetre-sized lava clasts may be wrapped by ash to form armoured lapilli, especially in UA6–10. Individual beds, each made by two couplets as at Secche di Lazzaro locality, thin laterally both upslope and along the valley sides (Fig. 7a), indicating the origin from pyroclastic density currents.

At this locality, the basal bed UA1 is thick, massive and chaotic, matrix supported, lithic-rich, showing a similar lithofacies to that shown by the lobe facies of UA1 and UA5 at Secche di Lazzaro. The matrix composes 60% of the deposit and consists of grey coarse-ash. The coarse fraction is up to 40% in volume and made by variably altered multilithologic, poorly sorted lithic fragments of lava. Light-coloured, vesicular pumice lapilli ranging between 1 mm and 3 cm in diameter are present. UA has a maximum thickness of 80 cm and it pinches out laterally along the flanks of the paleo-valley.

UB at Punta Lena is more than 7 m thick and is composed of at least four aggradational subunits. Individual beds are matrix-supported, massive, from chaotic to diffusely stratified, and show a reverse graded base. The ash is blocky and vesicular shards, crystal fragments and small lava lithic fragments. The coarse fraction can be up to 25–30% and is made of armoured lithic fragments up to 5 cm in diameter and multilithologic lava lithic clasts up to 40 cm in diameter. Light coloured pumice lapilli up to 2 cm in diameter are common (Fig. 8a). The top division of UB is characterised by well developed cross-stratification, which indicate a forestepping–backstepping stacking pattern (De Rita et al. 1998) (Fig. 8b), and suggests the emplacement from pulsatory pyroclastic density currents. Flow direction at this locality, as deduced by such paleo-flow indicators is towards the SE, i.e. seaward.
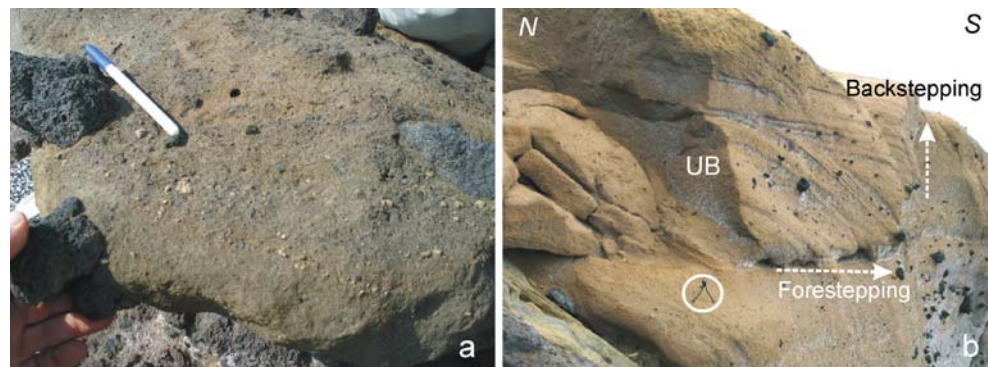
Semaforo Punta Labronzo locality

Semaforo Punta Labronzo is situated at the western tip of Stromboli (Fig. 1). At this locality the SDL deposits overlie Neostromboli lava. The deposit is a maximum of 6 m thick, is matrix-supported, chaotic and massive (Fig. 9a). The grey ash matrix constitutes 80–90% of the deposit, and in places it is vesiculated. The ash is bimodal, with ∼50% of fine ash (10–100 μm size), mostly made by blocky and hydrated glass shards and 50% coarse ash (0.5–2 mm size) made of sub-rounded multilithologic lava and crystal fragments. The coarse fraction is made of multilithologic and variably altered lava fragments with maximum diameter of 30 cm. Rare, light coloured pumice lapilli are present. Unidirectional grass prints at the base of the deposit indicate a northward direction of emplacement. This deposit is interpreted as the lahar associated with the SDL succession and therefore correlated with UC, although the lack at this locality of the underlying UA and UB units makes the correlation somewhat uncertain.

380 metres a.s.l. path toward the Pizzo sopra la Fossa

The SDL deposits crop out discontinuously between 300 m and 380 m a.s.l. along the path from Semaforo Punta Labronzo to the Pizzo sopra la Fossa (Fig. 1). The best outcrop is at 380 m a.s.l. where the succession dips 24°–N270° (Fig. 9b). The outcrop rests on Neostromboli lava. At this locality, SDL is marked at the base by 60 cm of plane-parallel stratified ash beds. The ash represents more than 90% of the deposit and consists of grey-yellow blocky and vesicular shards smaller than 0.0625 mm in size. Accretionary and armoured lapilli (<1 cm) are abundant. Subordinate centimetre-sized lava lithic clasts and scoria are dispersed in the ash matrix. Within this succession, two beds are markedly different. At the base, a 12-cm-thick layer (LQA) contains up to 40% sparsely porphyritic very vesicular light coloured pumice dispersed in a grey-ash matrix. At 40 cm from the base, an 8-cm-thick layer is present (LQB), massive to faintly stratified, indurated, made by grey ash with abundant blocky shards and

Fig. 8 **a** Light coloured pumice lapilli may constitute up to 1% of *UB*. **b** forestepping–backstepping stacking pattern in the top portion of *UB* at Punta Lena. Camera-tripod 30 cm height for scale

Fig. 9 a Massive and chaotic, matrix-supported, clast-rich lithofacies of SDL at Semaforo Punta Labronzo locality. This facies is interpreted as a syn-eruptive lahar unit and correlated to UC. **b** SDL deposit at 380 m a.s.l. path towards the Pizzo sopra la Fossa

fragments of clinopyroxene, biotite and plagioclase and sparse (max 5%) lava fragments. Cross-lamination shows a flow direction toward the NNW. LQB has similar characteristics to level UA5 at Secche di Lazzaro and Punta Lena.

The top of the outcrop consists of a 40 cm thick matrix-supported, massive, poorly sorted deposit. The matrix represents 70–75% of the deposit, and is composed of grey ash and 0.8 cm diameter accretionary lapilli. The coarse fraction represents 25–30% of the deposit, and is composed of black lava lithic lapilli and blocks with maximum diameter of 30 cm. On the top of this level, a channel is filled with epiclastic material and the succession is overlain by spatter bombs from the 1930 eruption.

Anisotropy of Magnetic Susceptibility (AMS)

Sampling and methods

The study of the flow directions of the pyroclastic units was performed by AMS analysis of the ash-rich matrix of the investigated deposits. We sampled the SDL deposit at the type locality along two sections, one parallel and one perpendicular to the coastline. In some cases, we sampled the same unit in different paleotopographic conditions. This sampling strategy was applied in order to study how different paleotopographic geometries can control the emplacement processes of volcanic units.

A total of 12 sites (207 measured samples) were sampled in units UA and UB. Among these, 3 sites were sampled orthogonal to the coastline and 9 sites parallel to the coastline (Table 1). Sites are labelled as follows: "S" (=Stromboli), then three characters related to the sampled level or unit (e.g. "UA1" means level A1), followed by a suffix "or"=orthogonal to the coastline, or "pl"=parallel to the coastline. In one case, we add another character to indicate a site sampled in veneer ("V") or in a lobe ("L") facies for the same level. Along the section orthogonal to the coastline, we sampled from bottom to top the levels UA1, UA5 and unit UB, corresponding to the sites SUA1or, SUA5or and STB-1or, respectively. Along the section parallel to the coastline we sampled the levels UA1,

Table 1 List of anisotropy factors calculated for each site

Site	N	K_m	L	F	P	T	D, I (K_{max})	D, I (K_{min})	E_{2-3}	E_{1-2}
SUA1pl	13	12.4 (0.2)	1.013 (0.006)	1.020 (0.004)	1.033 (0.006)	0.222 (0.233)	272, 15	48, 68	5	14
SUA1or	11	10.1 (1.9)	1.011 (0.008)	1.029 (0.010)	1.041 (0.011)	0.454 (0.294)	314, 2	56, 78	12	24
SUA5Vpl	30	14.5 (0.5)	1.001 (0.002)	1.064 (0.018)	1.068 (0.018)	0.957 (0.060)	35, 1	130, 85	2	32
SUA5or	8	12.0 (1.6)	1.012 (0.004)	1.028 (0.015)	1.041 (0.017)	0.393 (0.139)	133, 12	251, 66	37	12
SUA5Lpl	24	13.4 (2.8)	1.009 (0.009)	1.013 (0.009)	1.022 (0.014)	0.150 (0.363)	196, 4	327, 84	16	17
SUA5Cl	10	14.5 (1.6)	1.004 (0.010)	1.033 (0.010)	1.038 (0.018)	0.762 (0.223)	156, 13	3, 75	8	44
SUB-1pl	11	5.85 (0.3)	1.004 (0.002)	1.024 (0.005)	1.029 (0.007)	0.711 (0.104)	200, 8	30, 82	10	12
SUB-2pl	25	6.55 (0.4)	1.004 (0.003)	1.015 (0.003)	1.019 (0.004)	0.613 (0.193)	7, 2	109, 80	6	14
SUB-3pl	14	7.78 (0.2)	1.004 (0.002)	1.019 (0.002)	1.018 (0.002)	0.640 (0.143)	331, 14	124, 74	9	12
SUB-4pl	28	6.84 (1.0)	1.007 (0.002)	1.021 (0.005)	1.028 (0.005)	0.516 (0.171)	334, 6	145, 84	3	6
SUB-5pl	13	7.77 (0.3)	1.002 (0.001)	1.014 (0.002)	1.017 (0.002)	0.699 (0.133)	337, 6	118, 82	5	44
SUB-1or	20	7.32 (1.6)	1.006 (0.003)	1.021 (0.006)	1.026 (0.007)	0.537 (0.263)	180, 1	278, 87	6	39

The lines show the arithmetic means of the individual parameter values for each site (standard deviation in parentheses).
N measured samples, D azimuth, I inclination in degrees
$K_m=(K_{max}+K_{int}+K_{min})/3$ (magnetic susceptibility, in 10^{-3} units); $L=K_{max}/K_{int}$; $F=K_{int}/K_{min}$; $P=K_{max}/K_{min}$ (Jelinek 1976); $T=2(\eta_2 - \eta_3)/(\eta_1 - \eta_3) - 1$ (shape parameter; Jelinek 1976); $\eta_1=\ln K_{max}$; $\eta_2=\ln K_{int}$; $\eta_3=\ln K_{min}$; $\eta=(\eta_1+\eta_2+\eta_3)/3$; E_{2-3} and E_{1-2} are semi-angles of the 95% confidence ellipses around the principal susceptibility axes (derived from Jelinek 1976)

UA5 in two sites (in veneer and in lobe facies), corresponding to the sites SUA1pl, SUA5Vpl, SUA5Lpl. Along the same section we sampled consecutively the unit UB in five sites from the bottom to the top, corresponding to the sites SUB-1pl, SUB-2pl, SUB-3pl, SUB-4pl, SUB-5pl. This subdivision is not referred to a different facies of the unit UB. Moreover, in this section the level UA5 was also sampled on the top of a lava clast incorporated into the deposit. This site is called STA5Cl, where "Cl" means lava clast.

The AMS was measured by a KLY3 kappabridge at Roma Tre University. AMS is defined by a second rank symmetric tensor and is represented by an ellipsoid with the principal axes $K_{max} > K_{int} > K_{min}$. The results are projected on an equal-area projection, using the Jelinek (1976) statistics, and interpreted in terms of flow directions. Several parameters (T, P, see Table 1) are also used to describe the shape of the AMS ellipsoids. The T shape parameter may vary from −1 (perfectly prolate ellipsoid, $K_{max} > K_{int}$ and K_{min}) to +1 (perfectly oblate ellipsoid, K_{max} and $K_{int} > K_{min}$), while $T = 0$ corresponds to a triaxial ellipsoid. The magnetic lineation ($L = K_{max}/K_{int}$) and foliation ($F = K_{int}/K_{min}$) at sample and site scales are defined as the K_{max} direction and the plane normal to the K_{min}, respectively.

The definition of the direction and the sense of the flow by AMS in pyroclastic deposits is not always obvious. Commonly, the flattening (magnetic foliation) of the AMS ellipsoid is parallel to the stratification (or layering), and the elongation of the ellipsoid (magnetic lineation) is parallel to the flow direction (Fig. 10a). In some cases, the magnetic

lineation is orthogonal with respect to the flow direction inferred by field indicators (Fig. 10b). This particular spatial arrangement could be related to the rolling and saltating effect of the magnetic grains within the flow and can produce misleading interpretation of magnetic data in terms of flow direction (Ort et al. 2003 and references therein). For this reason, we prefer to use the K_{min} plunge direction and the imbrication of magnetic foliation to infer the mean direction and the sense of the flow respectively (Tarling and Hrouda 1993; Zanella et al. 1999; Porreca et al. 2003; Fig. 10c,d). Moreover, in order to avoid apparent flow direction, the imbrication of the magnetic foliation is interpreted with respect to the paleotopographic geometry, as shown in Fig. 10c,d.

Furthermore, besides the low-field AMS measurements at room temperature, we used high-field AMS measurements in order to discriminate the paramagnetic and ferrimagnetic contribution to the AMS fabric, which is a fundamental requirement to interpret AMS results in terms of mineral preferred orientation and flow directions. High-field measurements were performed in 9 selected samples from the different stratigraphic levels from the SDL section, with a high-field torque magnetometer (Bergmüller et al. 1994) applying the methodology used by Martin-Hernandez and Hirt (2001). No hematite is present in our samples and distinction between ferrimagnetic and paramagnetic contributions was therefore possible by applying magnetic fields up to 1800 mT. The high-field magnetic measurements were performed in the ETH paleomagnetic laboratory at Zurich.
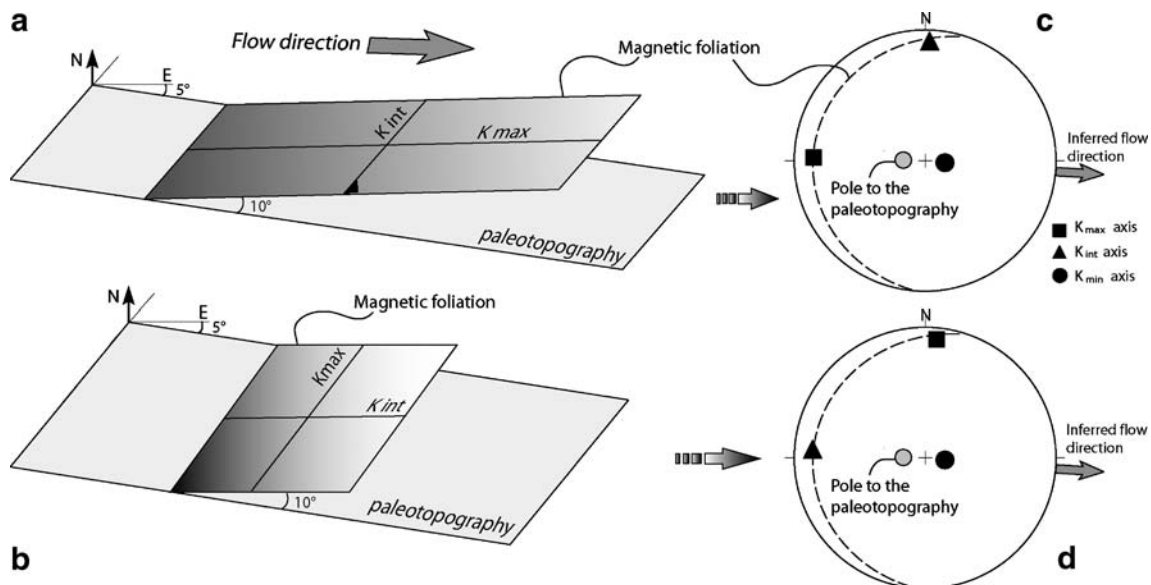

Fig. 10 Conceptual model for imbrication of magnetic foliation of two ideal cases. **a** Magnetic foliation can be imbricated with K_{max} axis oriented parallel and **b** orthogonal to the flow direction, and the related

c, **d** stereoplots of AMS axes. Note the same orientation of magnetic foliation and inferred flow direction in both cases
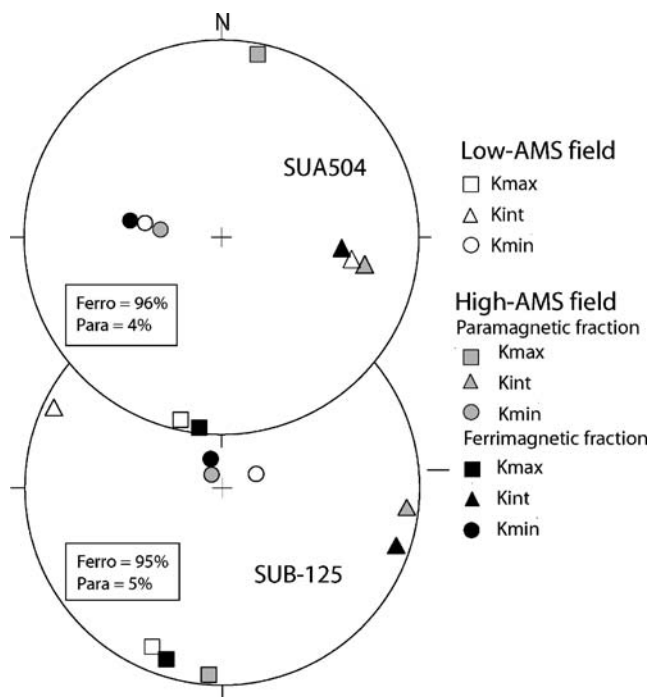
Fig. 11 Principal axes of the low-field (*white symbols*) and paramagnetic and ferrimagnetic components to the high-field magnetic anisotropy (*grey* and *black symbols*, respectively), in specimens characterised by high contributions of ferrimagnetic minerals. The percentages of ferrimagnetic (*Ferro*) and paramagnetic (*Para*) contributions are reported into the insets. Data are shown on equal area, lower hemisphere projections in geographic coordinates. Note the good agreement between the orientations of the paramagnetic and ferrimagnetic fractions

Magnetic fabric results

High-field data show that, in most of the samples, the magnetic anisotropy is entirely controlled by the ferrimagnetic fraction. The paramagnetic fraction only contributes a few percent to the total AMS (see Fig. 11). However, in all samples, the principal axes of both sub-tensors (paramagnetic and ferrimagnetic) coincide with those of the low-field AMS. The high-field AMS indicates that ferrimagnetic minerals (magnetite and titanomagnetite) control the magnetic fabric and, in the cases where the paramagnetic minerals also contribute to the AMS, they show the same orientation as the ferrimagnetic minerals (Fig. 11).

The magnetic susceptibility (K_m in Table 1) values range from 5.85 to 14.5×10^{-3} SI. The values measured for the sites sampled in the UA are higher than those of the UB, indicating a major amount of ferrimagnetic grains in the UA (Table 1).

The shape of the AMS ellipsoids is variable from triaxial to oblate shape (T parameter in Table 1). A different shape of the AMS ellipsoid has been measured in the different facies. Veneer facies show oblate ellipsoid shapes, whereas lobe facies show not well defined shapes. As an example, the thin veneer facies from level UA5 (site SUA5Vpl)

shows a well defined oblate ellipsoid, whereas the massive lobe facies shows a triaxial ellipsoid with a low anisotropy degree (Fig. 12a). This difference could be due to different emplacement mechanisms of the deposits and we will discuss this aspect in the next paragraph. The anisotropy degree (P) values range between 1.017 and 1.068, which are typical values for pyroclastic flow deposits. The highest values were measured in the UA1 and UA5 beds. Values of the P parameter in UB are higher just above the main stratigraphic discontinuities (dashed lines in Fig. 12b) which represent small discontinuities in sedimentation. By contrast, in the middle and upper parts of individual depositional units, the P values are lower and the AMS ellipsoid is not well defined (Fig. 12b). The magnetic fabric is better defined at the base depositional units, likely in response of higher shear.

The AMS ellipsoids are generally well defined (e.g. the examples of Fig. 13a,b,c), with the K_{min} axes tightly clustered and close to vertical, whereas K_{max} and K_{int} are either clustered (Fig. 13a,b) or weakly dispersed within the foliation plane (Fig. 13c), which is slightly dipping or sub-horizontal.

Almost all sites are characterised by a magnetic foliation which dips slightly upslope with respect to the topography (i.e. respect to the base), whereas the magnetic lineation is oriented downdip with respect to the foliation plane (Fig. 13b). On the other hand, the sites sampled in the basal layer UA1 show a magnetic foliation dipping downslope and a magnetic lineation oriented E–W (Fig. 13a). In this case, the orientation of magnetic foliation with respect to the sub-horizontal paleotopography suggests a flow direction from WSW to ENE (Fig. 13a) and then towards the volcano slope.

Inferred flow directions and implication on depositional mechanisms of the SDL pyroclastics

The SDL deposits were interpreted by Bertagnini and Landi (1996) as debris flow deposits interbedded with plane-parallel fall layers (ash-rich and accretionary lapilli layers), generated by a phreatomagmatic eruption. We define the emplacement mechanism and flow directions of these deposits by examining the magnetic fabric of the fine matrix.

In all cases well defined magnetic foliation and magnetic lineation are found, suggesting that each sampled unit was emplaced by pyroclastic density currents, in agreement with the stratigraphic and sedimentological characteristics discussed above. We recall that results from high-field measurements show that AMS is mostly controlled by the ferromagnetic fraction (Fig. 11), and therefore the flow directions deduced by AMS results is related to the preferred orientation of magnetite grain. However, the same orientation has been also measured for the paramagnetic

Fig. 12 a P vs T diagram for the sites SUA5Lpl and SUA5Vpl; **b** Variation of P parameter with the stratigraphic height for the UB unit. The *dashed lines* indicate the height of stratigraphic discontinuities within UB (cf Fig. 6)
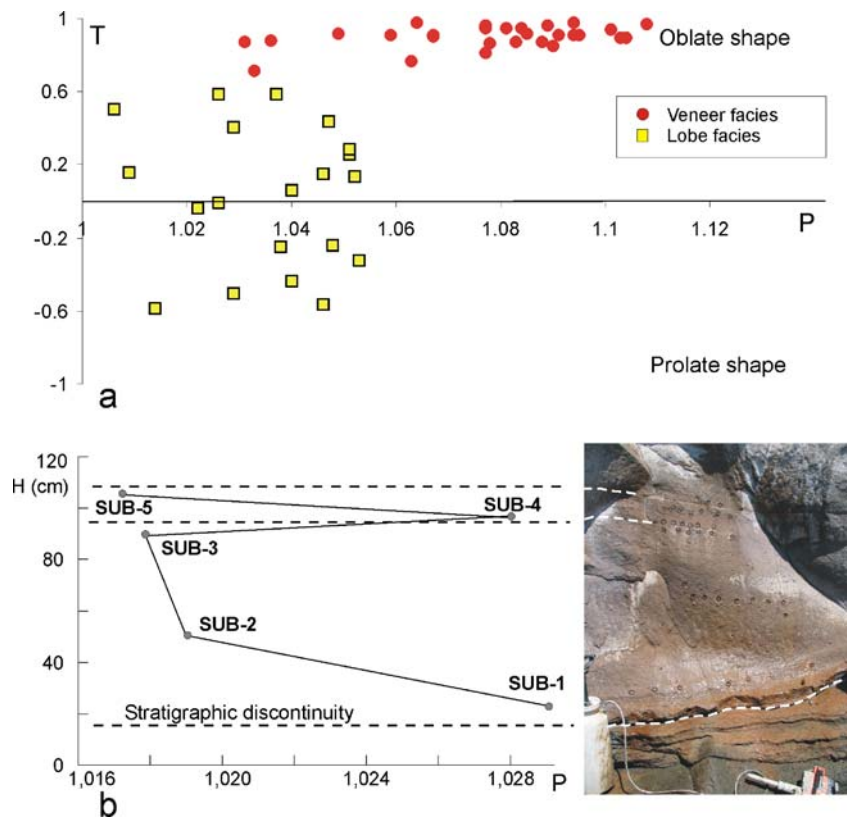
sub-tensor which is related to paramagnetic minerals (i.e. biotite, Fe-rich silicates), suggesting that AMS results indeed reflect the preferred orientations of the different mineral fractions in the sampled rocks. Furthermore, the subparallel orientation of minerals with a different shape also suggest to exclude that mechanism as rolling of elongated particles which could adjust minerals orthogonal to the flow, be a suitable mechanism to explain the observed AMS results. Conversely, our results show that there is not such behaviour in the flow and that the mineral preferred elongation evidenced by the AMS results is parallel to the flow directions.

The orientations of magnetic foliation can then be used as flow indicators and compared with the field indicators such as clast imbrications, sedimentary structures (e.g. dunes, anti-dunes, low angle cross laminations), and imbrication of unburned cane pieces. These field indicators measured in the UA and UB units generally suggest a flow direction from NNE toward SSW (examples in Figs. 5a and 13b), i.e. from the summit vent toward the sea.
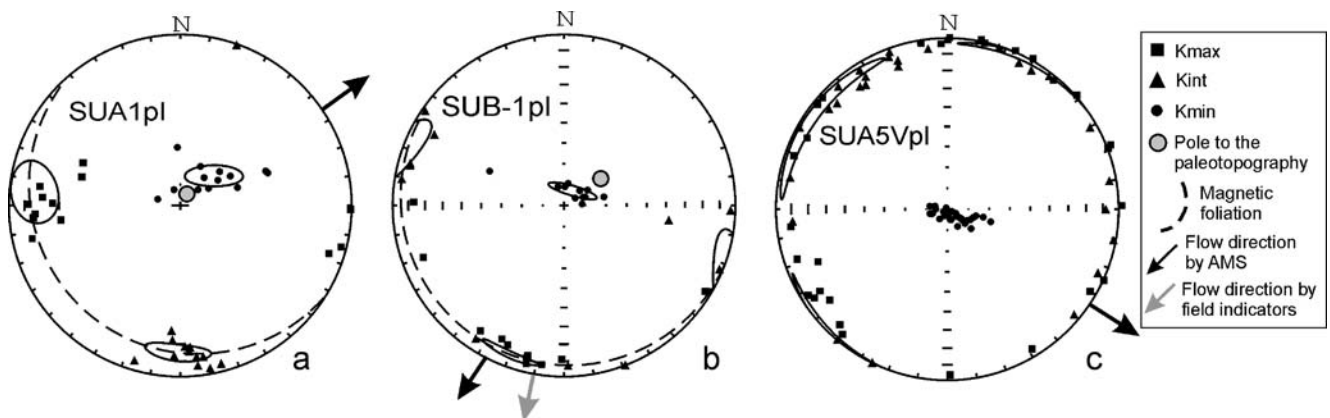

Fig. 13 Equal-area projections of principal magnetic axes of three representative sites: **a** the basal level UA1; **b** the level UB-1; **c** veneer facies of UA5. The coastline is oriented WNW–ESE, the crater is located toward the NE and the sea toward the S
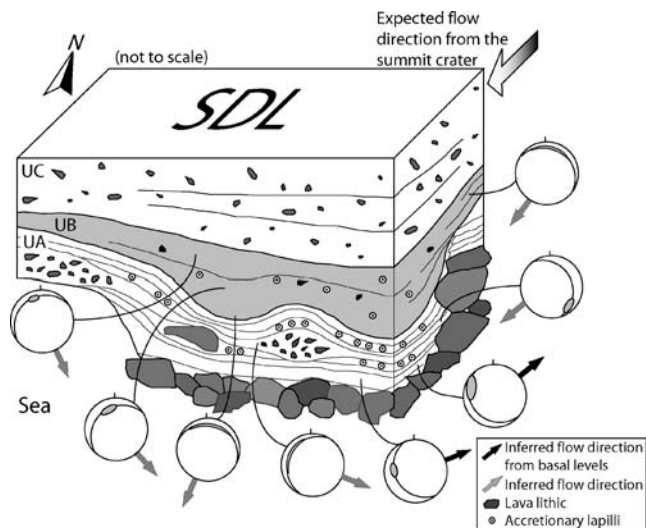
Fig. 14 Block diagram of *SDL* deposit with the inferred flow directions obtained by AMS data. *Symbols* in equal-area projections: *great circles* indicate magnetic foliation; *grey ellipses* indicate the ellipses of confidence of magnetic lineation. The inferred flow direction are given by sense of imbrication of magnetic foliation. Note the unexpected uphill flow direction (*black arrows*) for the basal part of *SDL* deposits

The flow directions obtained by AMS data are summarised in Fig. 14. It is worth noting that the imbrication of the magnetic foliation and the plunge of K_{min} (that is the pole of magnetic foliation) from the basal part of unit UA suggest an unexpected provenance of the pyroclastic density current, from SW toward NE, i.e. uphill. The rest of unit UA shows a flow direction variable from NE toward SW and from NW toward SE (Fig. 14). The unit UB of the section shows a sense of the flow from NW to SE (downhill). Variations in flow direction between the base and the rest of the unit UB also occurred, indicating a variation of the flow direction during the deposition. In particular, the inferred flow direction is from NE toward SW at the base and from NW to SE for the rest of the unit. In this case, the basal part of the flow is not influenced by the paleotopography because it was very energetic and able to climb the topography barriers, whereas the emplacement of the rest of the pyroclastic current was controlled by the topography. Moreover, for this unit, anisotropy degree (P) varies vertically, with highest P values in correspondence of stratigraphic discontinuities (Figs. 6 and 12b). This suggests that the magnetic fabric is well defined when the shear is maximum during waxing phases of the pyroclastic current. The upward poorer definition of the AMS ellipsoid (Fig. 12b) indicate a larger dispersion of the magnetic grains likely related to deposition from a waning current.

The magnetic fabric data demonstrate that the shape of AMS ellipsoids is different in the various sampling facies. This is because the emplacement of the pyroclastic density current was more strongly influenced by the irregularities of the paleotopography more than the transport system. In the same unit we found different facies related to paleotopographic location. The facies channelled into a paleo-valley are characterised by high sedimentation rate where the magnetic grains have no time to arrange along the flow, whereas the veneer facies is well organised and characterised by a low sedimentation rate. The magnetic data reflect these different features in the emplacement processes as shown in Fig. 12a.

Discussion

The Secche di Lazzaro pyroclastics (SDL) is made of three main units: UA, the lower unit, is made of parallel- to cross-stratified, ash-supported and accretionary lapilli-rich thin beds; UB, is massive to poorly stratified, ash-supported, accretionary and armoured lapilli-bearing, and valley ponded; UC, the topmost unit, is made of massive and lithic-rich, metre-thick beds. The SDL is consistently made of blocky and vesicular glass shards and abundant accretionary and armoured lapilli, which, in agreement with Bertagnini and Landi (1996), confirm the phreatomagmatic origin, a very rare mechanism of fragmentation at Stromboli.

First we discuss the mechanisms of emplacement of SDL. Hornig-Kjarsgaard et al. (1993) and Bertagnini and Landi (1996) interpreted the succession as emplaced by fallout for the stratified accretionary lapilli-rich beds of UA, and by mudflows for the thicker and massive divisions (which correspond to our UA1, UA5, UB and UC). We have discussed in the previous sections that the stratigraphic, facies and magnetic characteristics are instead consistent with an origin from low temperature (Porreca et al. 2006), more or less dilute, pulsatory pyroclastic density currents for units UA and UB, and from lahars for unit UC.

The succession starts with level UA0 which fills the empty spaces in between the blocks of the paleobeach of Neostromboli (Fig. 3a). The presence of cane moulds admixed with accretionary lapilli and ash (Fig. 3a) suggests the passage of a very dilute pyroclastic density current over the very permeable paleobeach lava cobbles and blocks. Eddies may have formed within these cavities, forming concentrations of ripped up canes upcurrent, and segregating the clast supported accretionary-lapilli deposit (Fig. 3a), from which the ash matrix was elutriated by the overflowing current.

Individual beds constituting UA1–UA10 are characteristically made by a distinct couplet of layers: basal layer (UA$_b$) and top layer (UA$_t$), described above (Fig. 3c). Figure 15 illustrates a possible model of the pyroclastic density current from which individual layers described for UA were emplaced. UA$_b$ layers were emplaced from the

Fig. 15 Schematic model of emplacement of the pyroclastic density current related to UA in two distinct layers (UA_b vs. UA_t). See the text for explanation
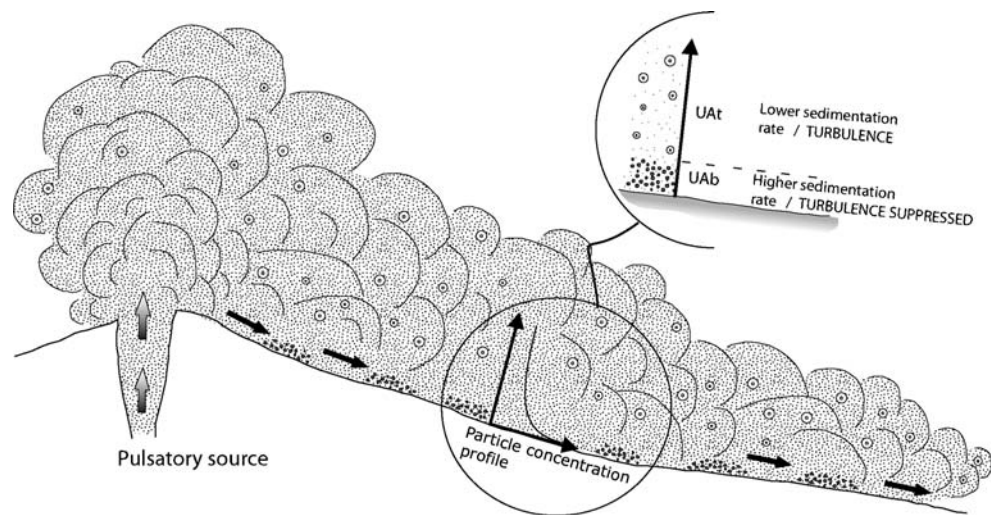
early, basal, higher concentration zone, characterised by a higher sedimentation rate. These characteristics account for the massive to faintly stratified facies of UA_b, as the high sedimentation rate would suppress turbulence (Branney and Kokelaar 2002). Furthermore, in a low temperature current, a high sedimentation rate would promote the trapping of vapour in the deposit (Lorenz 1974) and therefore explains both the presence of vesiculation in the ash and the sticky (mantling) behaviour of UA_b with respect to topography. The accretionary lapilli-rich UA_t can be generated in a more dilute traction zone where ash can aggregate to form accretionary lapilli during the turbulent transport (Cas and Wright 1987). The repetitive succession of beds UA1–UA10 can be interpreted as related to a pulsatory current, in which each pulse deposited a couplet of UA_b–UA_t. This explains the formation of progradational dunes that involve the whole UA1–UA10 package (Fig. 3b). Despite the low concentration of the pyroclastic density currents at the Secche di Lazzaro locality, the package UA1–UA10 is associated with considerable erosional capacity. UA1–UA4 are commonly squeezed in at the base of blocks, suggesting that early deposition underneath metre-sized lava blocks may have destabilised the blocks, which in several occurrences appear rotated, pushed, lifted and imbricated (Fig. 5a). UA5 is commonly plastered laterally and UA6–UA10 are laid on top. The erosional capacity may account for the development of the lithic-rich lobe facies of UA1 and UA5, which may have bulked during deposition and/or slumped, due to condensed vapour lubrication, from the steep upper reaches of the volcano.

The transition from UA to UB is without a significant time-break, as there is no erosional surface whatsoever in between (Figs. 6a and 7a). UB is thicker, more massive, and more valley-ponded. These characteristics suggest an increase in sedimentation rate with time (Branney and Kokelaar 2002). Variation of AMS fabric across layering of UB (Fig. 12b), together with the forestepping–backstepping

stacking patterns present at Punta Lena (Fig. 8b), suggest a pulsatory nature of the pyroclastic density current also for UB. The stratigraphic contact between UB and UC is almost concordant and suggests that the lahar mobilisation started immediately after the end of the eruption.

Now we discuss the origin of the SDL phreatomagmatic pyroclastics. Hornig-Kjarsgaard et al. (1993) interpreted the succession as locally derived from a vent located probably offshore, because they considered the Secche di Lazzaro pyroclastics to only crop out on the southern coast of Stromboli. However, this interpretation is not supported, as 1) there is no evidence of any submarine centre (Gabbianelli et al. 1993), and, more convincingly, 2) the deposits are distributed all around the island (Fig. 1). Bertagnini and Landi (1996) noted the stratigraphic "coincidence" between the Neostromboli sector collapse and the SDL eruption as well as its almost unique characters within the entire history of Stromboli and called for a causal relationship between the two. Unfortunately, there are no stratigraphic sections where the deposits of the debris avalanche are in outcrop because they were directed seaward, so it is impossible to assess objectively the relationship between the SDL eruption and the lateral sector collapse event.

A first speculation can be made about the largely phreatomagmatic character of SDL. At present the ground-water table at Stromboli is lower than the magmastatic level in the conduit (Revil et al. 2004), and there is no explosive magma–water interaction. This suggests that an established conduit filled up with magma is able to heat up and push away the surrounding groundwater and no interaction is generated. The style of activity of the Neostromboli period deduced from the stratigraphy (Hornig-Kjarsgaard et al. 1993) was remarkably similar to that witnessed today, so it is likely that Neostromboli had a high magmastatic level producing open conduit conditions and intermittent mild explosions and effusion, similarly to the present style of activity. By contrast, an efficient magma–water interaction

can be achieved when a rising batch of magma encounters a water body during ascent (Heiken and Wohletz 1985, 1991; Wohletz 2002). It cannot be excluded that in the past, the magmastatic level may have been at some stages lower then the groundwater table, creating favourable conditions for explosive magma–water interaction to occur. We believe, however, that the obvious scenario for explosive magma–water interaction at Stromboli is, in agreement with the suggestion of Bertagnini and Landi (1996), the lateral sector collapse, which would allow at the same time the sudden decompression of the magma and likely its vesiculation and fragmentation and the access of the external water to the vent, mobilised by the decapitation of the volcano.

With this in mind, flow directions inferred from AMS at Secche di Lazzaro locality are very intriguing. The basal part of SDL (UA0 and UA1), only at this locality bears an inferred flow direction from the sea toward the volcano (Fig. 14). Upward, the paleoflow directions change and show a provenance from the summit region. In all the other investigated sites, inferred paleoflow directions are directed downhill, that is, on the volcano scale, radially from the summit vent. We believe that the mechanism responsible for the emplacement of UA0–UA1 can be related to the radial spreading of pyroclastic base surges at the onset of the eruption, which were able to laterally expand and flow around the shoulder of the sector collapse scar to reach the Secche di Lazzaro-Ginostra coastline (Fig. 16). Part of the lateral expansion of the surge may relate to the sudden decompression of the magma and the access of water to the conduit as a consequence of the sector collapse. A similar behaviour has been reconstructed for the 8th and 20th May
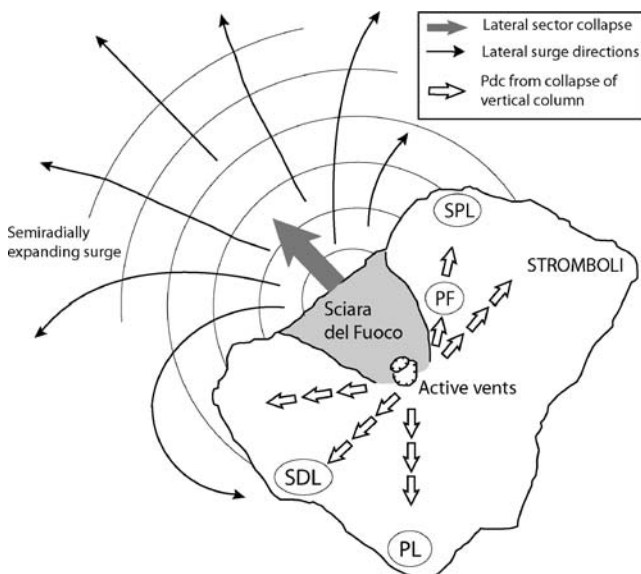
1902 eruptions of Mt Pelée (Martinique), where flows developed a lateral component strong enough to destroy St. Pierre located along the coast, and to spread uphill along lateral gullies (Fond Canonville) (Fisher et al. 1980; Fisher and Heiken 1982). Similarly, uphill re-direction of dilute pyroclastic density currents are described at Montserrat (Druitt and Kokelaar 2002) and for 18th May 1980 lateral blasts at Mount St. Helens (Christiansen and Peterson 1981).

The radial downhill directed paleoflow directions inferred for the rest of the SDL stratigraphy (UA2–UA10, UB) can be associated with the collapse of pyroclastic density currents from a vertically directed eruptive column, established after the initial laterally spreading surge (white arrows in Fig. 16).

Considering that the Stromboli magma is not likely to produce domes and cryptodomes, like in the cases of the other above mentioned volcanoes, the trigger for the overpressurised initial surge could be sudden access of water to the volcanic conduit induced by decapitation of the volcano, along with decompression of the magma. The nature of the water involved is likely associated with the hydrothermal system (Bertagnini and Landi 1996), although seawater may be another ready available source.

A major shortcoming of the proposed model is the absence of any obvious tsunami deposit associated with the SDL. It would be expected that the debris avalanche of the sector collapse would have produced an important tsunami immediately after the collapse (e.g,. Bonaccorso et al. 2003; McMurtry et al. 2004). Some deposits on Stromboli have tentatively been associated with the Neostromboli sector collapse (Tanner and Calvari 2004), but bear no stratigraphic relations with the SDL deposits. Considering that, since the SDL emplacement, there have been no important changes of the coastline, as indicated by the paleobeach substrate at Secche di Lazzaro locality, the implication is that between the lateral sector collapse and the phreatomagmatic eruption enough time passed to allow the tsunami to wash out the coastline before the emplacement of the SDL succession. This elapsed-time can be quantified in the order of seconds to 1–2 min, according to velocities both measured and calculated for tsunami propagation in shallow water (e.g. La Rocca et al. 2004).

Fig. 16 Schematic reconstruction of eruption responsible for the SDL emplacement. SDL Secche di Lazzaro, PL Punta Lena, SPL Semaforo Punta Labronzo; PF Pizzo sopra la Fossa

Conclusions

The Secche di Lazzaro succession records a large phreatomagmatic eruption triggered by a catastrophic sector collapse of Stromboli at ~5 ka. The integration of stratigraphic, facies and magnetic fabric data allow us to propose an eruptive and emplacement scenario for the Secche di Lazzaro pyroclastics. During the early stages of

the eruption, low-temperature, low density pyroclastic currents were generated in pulses. Sudden and catastrophic water/magma interaction likely triggered a laterally spreading surge able to move around topographic barriers, wrapping around the shoulder of the collapse scar. This surge deposited the thin surge deposits of units UA0 and UA1 that show paleocurrent directions from the sea uphill. Subsequently, the eruption continued by establishing a vertical eruptive column able to generate pyroclastic currents that radially spread along the volcano slopes and which are characterised by thicker and more massive facies and downhill-directed paleoflow directions (units UA2–UA10, UB). Immediately post-eruptive remobilisation of ash from the volcano cone emplaced thick lahar deposits on the lower reaches (unit UC).

The consistent high fragmentation degree of the Secche di Lazzaro pyroclastics indicates that the efficiency of magma—water interaction did not change drastically during the eruption, suggesting a steady availability of water to access the magma conduit after decapitation of the volcano.

References

Barberi F, Rosi M, Sodi A (1993) Volcanic hazard assessment at Stromboli based on review of historical data. Acta Vulcanol 3:173–187

Bergmüller F, Bärlocher C, Geyer B, Grieder M, Heller F, Zweifel P (1994) A torque magnetometer for measurements of the high-field anisotropy of rocks and crystals. Meas Sci Technol 5:1466–1470

Bertagnini A, Landi P (1996) The Secche di Lazzaro pyroclastics of Stromboli volcano: a phreatomagmatic eruption related to the Sciara del Fuoco sector collapse. Bull Volcanol 58:239–245

Bogoyavlenskaya GE, Braitseva OA, Melekestsev IV, Kiriyanov VY, Miller CD (1985) Catastrophic eruptions of the directed-blast type at Mount St. Helens, Bezymianny and Shiveluch volcanoes. J Geodyn 3:189–218

Bonaccorso A, Calvari S, Garfi G, Lodato L, Patanè D (2003) Dynamics of the December 2002 flank failure and tsunami at Stromboli volcano inferred by volcanological and geophysical observations. Geophys Res Lett 30: DOI 10.1029/2003GL017702

Branney MJ, Kokelaar P (2002) Pyroclastic density currents and the sedimentation of ignimbrites. In: Branney MJ, Kokelaar P (eds) (eds) Pyroclastic density currents and the sedimentation of ignimbrite. vol. 27. Geological Society, London, pp 1–138

Cas RAF, Wright JV (1987) Volcanic successions modern and ancient. Allen and Unwin, London, p 528

Christiansen RL, Peterson DW (1981) Chronology of the 1980 eruptive activity. In: Lipman PW, Mullineaux DR (eds) The 1980 eruptions of Mount St. Helens, Washington. USGS

Professional Paper, 1250, U.S. Government Printing Office, Washington, DC, pp 1–844

De Astis G, Ventura G, Vilardo G (2003) Geodymanic significance of the Aeolian volcanism (Southern Tyrrhenian Sea, Italy) in light of structural, seismological and geochemical data. Tectonics 22:1040

De Rita D, Giordano G, Milli S (1998) Forestepping–backstepping stacking pattern of volcaniclastic successions: Roccamonfina volcano, Italy. J Volcanol Geotherm Res 80:155–178

Druitt TH, Kokelaar BP (eds) (2002) The eruption of Soufriere Hills Volcano, Montserrat, from 1995 to 1999. Geological Society, London, (Geol Soc Mem 21)

Ferrari L, Manetti P (1993) Geodynamic framework of the Tyrrhenian volcanism: a review. Acta Vulcanol 3:1–10

Fisher RV, Smith AL, Roobol MJ (1980) Destruction of St. Pierre, Martinique by ash-cloud surges, May 8 and 20, 1902. Geology 8:472–476

Fisher RV, Heiken G (1982) Mt. Pelee, Martinique: May 8 and 20, 1902, pyroclastic flows and surges. J Volcanol Geotherm Res 13:339–371

Gabbianelli G, Romagnoli C, Rossi PL, Calanchi N (1993) Marine geology of the Panarea–Stromboli area (Aeolian Archipelago, Southeastern Tyrrhenian sea). Acta Vulcanol 3:11–20

Gillot PY, Keller J (1993) Radiochronological dating of Stromboli. Acta Vulcanol 3:69–77

Heiken G, Wohletz K (1985) Volcanic ash. Univeristy of California Press, Berkeley, p 246

Heiken G, Wohletz K (1991) Fragmentation processes in explosive volcanic eruptions. In: Fisher RV, Smith GA (eds) Sedimentation in volcanic settings. Society of Economic Paleontologists and Mineralogists, USA, pp 19–26 (Special Publications # 45)

Hornig-Kjarsgaard I, Keller J, Kobersky U, Stadlbauer E, Francalanci L, Lenhart R (1993) Geology, stratigraphy and volcanological evolution of the island of Stromboli, Aeolian arc, Italy. Acta Vulcanol 3:21–68

Jelinek V (1976) The statistical theory of measuring anisotropy of magnetic susceptibility of rocks and its application. Geophyzika, Brno, pp 1–63

Kokelaar P, Romagnoli C (1995) Sector collapse, sedimentation and clast population evolution at an active island-arc volcano: Stromboli, Italy. Bull Volcanol 57:240–262

La Berge RD, Giordano G, Cas RAF (2006) Syn-depositional deformation of a substrate produced by the shear force of a pyroclastic density current: an example from the Cimino Ignimbrite, Northern Lazio, Italia. J Volcanol Geotherm Res 158:307–320

La Rocca M, Galluzzo M, Saccorotti G, Tinti S, Cimini GB, Del Pezzo E (2004) Seismic signals associated with landslides and with a tsunami at stromboli volcano, Italy. Bull Seismol Soc Am 94–5:1850–1867

Lorenz V (1974) Vesiculated tuffs and associated features. Sedimentology 21:273–291

Martin-Hernandez F, Hirt AM (2001) Separation of ferrimagnetic and paramagnetic anisotropies using a high-field torsion magnetometer. Tectonophysics 337:209–221

McMurtry GM, Watts P, Fryer GJ, Smith JR, Imamura F (2004) Giant landslides, mega-tsunamis, and paleo-sea level in the Hawaiian Islands. Mar Geol 203:219–233

Ort MH, Orsi G, Pappalardo L, Fisher RV (2003) Anisotropy of magnetic susceptibility studies of depositional processes in the Campanian Ignimbrite, Italy. Bull Volcanol 65:55–72

Pasquaré G, Francalanci L, Garduño VH, Tibaldi A (1993) Structure and geologic evolution of the Stromboli volcano, Aeolian Islands, Italy. Acta Vulcanol 3:79–89

Porreca M, Mattei M, Giordano G, De Rita D, Funiciello R (2003) Magnetic fabric and implications for pyroclastic flow and lahar

emplacement, Albano maar, Italy. J Geophys Res 108:2264 DOI 10.1029/2002JB002102

Porreca M, Giordano G, Mattei M, Musacchio P (2006) Evidence of two Holocene phreatomagmatic eruptions at Stromboli volcano (Aeolian Islands) from paleomagnetic data. Geophys Res Lett 33: L21316 DOI 10.1029/2006GL027575

Revil A, Finizola A, Sortino F, Ripepe M (2004) Geophysical investigations at Stromboli volcano, Italy: implications for ground water flow and paroxysmal activity. Geophys J Int, 157:426–440

Ripepe M, Marchetti E, Ulivieri G, Harris AJL, Dehn J, Burton M, Calatabiano T, Salerno G (2005) Effusive to explosive transition during the 2003 eruption of Stromboli volcano. Geology 33:341–344

Romagnoli C, Kokelaar P, Rossi PL, Sodi A (1993) The submarine extension of Sciara del Fuoco feature (Stromboli Island): morphological characterization. Acta Vulcanol 3:91–98

Rosi M (1980) The island of Stromboli. Rend Soc Ital Mineral Petrol 36:345–368

Rosi M (1992) A model for the formation of vesiculated tuff by coalescence of accretionary lapilli. Bull Volcanol 54:429–434

Rosi M, Bertagnini A, Landi P (2000) Onset of the persistent activity at Stromboli volcano (Italy). Bull Volcanol 62:294–300

Selvaggi G, Chiarabba C (1995) Seismicity and P-wave velocity image of the southern Tyrrhenian subduction zone. Geophys J Int 121:818–826

Speranza F, Pompilio M, Sagnotti L (2004) Paleomagnetism of spatter lavas from Stromboli volcano (Aeolian Islands, Italy): Implications for the age of paroxysmal eruptions. Geophys Res Lett 31: L02607 DOI 10.1029/2003GL018944

Tanner LH, Calvari S (2004) Unusual sedimentary deposits on the SE side of Stromboli volcano, Italy: products of a tsunami caused by the ca. 5000 years BP Sciara del Fuoco collapse. J Volcanol Geotherm Res 137:329–340

Tarling DH, Hrouda F (1993) The magnetic anisotropy of rocks. Chapman & Hall, London, pp 1–217

Tibaldi A (2001) Multiple sector collapses at Stromboli volcano, Italy: how they work. Bull Volcanol 63:112–125

Wohletz K (2002) Water/magma interaction: some theory and experiments on peperite formation. J Volcanol Geotherm Res 114:19–35

Zanella E, Lanza R, De Astis G, Dellino P, La Volpe L (1999) Magnetic fabric and remanent magnetization of pyroclastic surge deposits from Vulcano (Aeolian Islands, Italy). J Volcanol Geotherm Res 93:217–236